



Research Article

Parametric oscillation and amplification with gate controlled capacitor-within-capacitor

H. Grebel¹ 

Received: 7 August 2020 / Accepted: 17 May 2021

Published online: 29 May 2021

© The Author(s) 2021 [OPEN](#)

Abstract

Parametric oscillators and parametric amplifiers are known for their ‘quiet’ operation and find new applications in quantum circuitry. A Capacitor-within-Capacitor (CWC) is a nested electronic element that has two components: the cell (e.g., the outer capacitor) and the gate (e.g., the inner capacitor). Here we provide analysis and experiments on diode-interfaced, CWC that exhibit parametric oscillations and parametric amplifications. By replacing the diode with a doped nano-graphene junction, we demonstrated a new structure whose doping may be electronically and chemically controlled. Advantages of these elements are in their simplicity, large relative capacitance change (of the order of 50%), separation of pump and signal channels and possibility for large integration.

Keywords Parametric Oscillation · Parametric Amplification · Graphene junctions · Capacitor within-Capacitor

1 Introduction

In equivalent circuit terms, capacitors may be connected in series (the overall capacitance becomes smaller than that of either capacitor), or in parallel (the overall capacitance is the sum of individual capacitances) [1]. Capacitors may take a simple form, such as two parallel plates, or a more complex structure of interdigitated electrodes [2]. Recently, a third possibility, a capacitor-within-capacitor (CWC), was considered [3]. Specifically, one capacitor, the gate capacitor, electronically controls the capacitance of a cell capacitor. The gate may be nested inside the cell (inner gate structure) or outside it (outer gate structure). Such a concept is general and may be applied to dielectric and super-capacitors alike. If the electrodes are made of 2-D films, such as graphene; voltage controlled charge doping of either electrode may be achieved in a rather simple manner [4].

Electrical parametric oscillators have been known for a long time [5]. In an electrical parametric oscillator, a

resonating circuit is interfaced with a nonlinear capacitor, or nonlinear inductor [6]. Modulation of the nonlinear element by a pump source at frequency ω_p and above some intensity threshold results in the generation of two frequency components: the signal at ω_s and an idler at ω_i . Conservation of energy dictates that, $\omega_p = \omega_s + \omega_i$. When the signal and the pump are in phase (or, shifted by π radians), then $\omega_s = \omega_i$ and the signal oscillates at half-frequency of the pump. Typically, a varactor, or a similar nonlinear capacitive element is used to realize the electrical circuit. Here, we take a somewhat different approach to realize a nonlinear capacitor (Fig. 1). One key advantage of parametric oscillators and amplifiers is their large signal-to-noise ratio without compromising low noise levels. This makes them very attractive to modern quantum circuits [6]. The relative large capacitance change and structural simplicity lends itself to a relatively easy fabrication of integrated circuits.

The paper is organized as follows: the General Concept and Design Considerations are first described. Theoretical

✉ H. Grebel, grebel@njit.edu | ¹Electronic Imaging Center, NJIT, Newark, NJ 07102, USA.



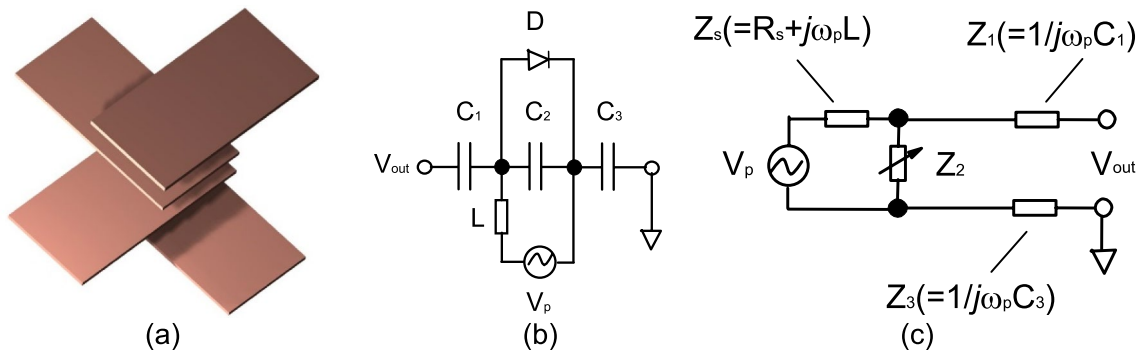


Fig. 1 **a** Schematics of the CWC. Four stripes of copper are placed one on top of each other and are separated by dielectric films. **b** The equivalent circuit. C–capacitor(s); D–diode; L–inductor.

c Thevenin equivalent: Z_2 is the capacitor impedance in parallel with the varying diode resistance, and Z_s is the sum of the source and inductor impedances

Considerations and a model are provided in section II. Methods and Experiments are provided in section III. Experimental Results and Discussions for the oscillator and amplifier are provided in section IV followed by the Conclusion section.

1.1 The general concept and design considerations

Consider an inner CWC structure and its equivalent circuit (Fig. 1a–c). A diode, placed across the gate capacitor [Ref. 3 and its SI section] provides for a voltage controlled element. Using Fig. 1b one may focus on the inner RLC circuit of the gate. We note that the pump source, V_p , has an output resistance; typically, $R_s = 50$ Ohms (Fig. 1c). The AC Thevenin equivalent impedance seen from the output when $V_p = 0$, with $R_s + \omega_p L \gg 1$, and $\omega_p C \ll 1$ may be approximated as $Z_{TH} \sim (Z_{C1} + Z_{C3}) + Z_{C2}$, where Z_{C1} is the impedance for the C_1 capacitor and so on. In the ideal case, if the diode is forward biased, then its resistance is small, thus bypassing C_2 . As a result, and if the capacitors are all the same, $Z_{TH}^F \sim j/(\omega_p C/2)$. If the diode is reversed biased, then, $Z_{TH}^R \sim j/(\omega_p C/3)$. The large capacitance change occurs when the AC pump signal oscillates near the diode break-in voltage (0.7 V for Si diode), or at the diode saturation voltage. Selection of the basic resonance pump frequency (in Hertz) is made through, $(f_p)^2 = (\omega_p/2\pi)^2 = (1/LC)/4\pi^2$. The amplification, and eventual oscillations will occur at $f_s \sim f_p/2$.

2 Theoretical considerations and modeling

Besides nonlinearities near the break-in region, a typical diode circuit exhibits nonlinearity when biased with either large negative amplitudes (the Zener effect), or large positive amplitudes (saturation effect). The effect at large positive biases happens when a small effective resistor, R , is

connected in series with a diode. This resistor could be the result of contacts or wires. The current–voltage equation for the circuit current becomes, $I_d = I = I_0 \{ \exp[(V - I \cdot R)/V_q] - 1 \}$, where I_0 is the dark current, V is the input voltage and $V_q = 26$ mV at room temperature. For a large input voltage and small resistances, the term $I \cdot R$ competes with the input V and the current becomes saturated. Thus, the transition from a quasi linear I – V curve to saturated curve is also a useful parametric oscillation region.

Let us look closely at the nonlinear capacitive response. An equivalent circuit model is shown in Fig. 1b. One may assume that the capacitance, C , between nearest pairs of plates is the same because the spacing and the dielectric materials are similar. As described before, the maximum nonlinear capacitance swing may reach 50%, between cell capacitance values of $C/3$ – $C/2$ when the gate capacitor is either open or short.

We start with the nonlinear equation for a pumped capacitor [7]. We assume that the capacitance of the cell (namely, the outer set of electrodes) depends linearly on the shunt resistance across the gate within some resistance region [3] : $C(R_{shunt}) \sim C_0(1 - R_{shunt}/R_0)$. Here C_0 is the cell capacitance without the shunt gate resistance and R_0 is a constant. From the diode equation for small currents (namely, ignoring the saturation region of the circuit), we can write for the effective diode resistance as a function of $V_p \equiv V_{pump}$

$$R_{eff} = (dI/dV_p)^{-1} = (V_q/I_0) \{ \exp(-V_p/V_q) \} \tag{1}$$

Combining, $C(V_p) \sim C_0(1 - (V_q/R_0 I_0) \exp(-V_p/V_q))$. Finally, $\Delta C/C_0 \sim (V_q/R_0 I_0) \exp[-(V_{p0}/V_q)] \sin(\omega_p t)$. As the voltage increases, the diode resistance decreases and the cell's capacitance increases.

The signal is set to the resonant frequency of this circuit, $\omega_s^2 = (1/LC)$. We write, $C = C_0 + \Delta C = C_0(1 + \Delta C/C_0)$ and $L = L_0 - \Delta L = L_0(1 - \Delta L/L_0)$ with $\Delta C/C_0 < 1$ and $\Delta L/L_0 < 1$.

Here L_0 and C_0 are associated with the non-modulated resonance frequency of the circuit. The nonlinear modulation of the gate between low and high shunt diode resistance affects the overall cell's capacitance and leads to, first, amplification which is followed by oscillations. Note the choice of a plus sign to the capacitance change; the capacitance increases upon a positive pump swing.

The effect of L on the effective permittivity of the cell is expected to be smaller than the capacitive effect since magnetic dipoles are smaller than electric ones. In addition, the outer electrodes are well separated and form only a partial current loop. We will ignore it for the sake of simplicity and write for the parametrization of the frequency through first order expansion,

$$\omega_s^2 \approx (1/L_0 C_0) (1 - \Delta C/C_0) (1 + \Delta L/L_0) \rightarrow (1/L_0 C_0) (1 - (V_q/R_0 I_0) \exp[-(V_{p0}/V_q) \sin(\omega_p t)]) \quad (2)$$

This is to be compared to a more traditional parametric oscillator,

$$\omega_s^2 \sim (1/L_0 C_0) (1 - bV_{p0} \sin(\omega_p t)) \quad (3)$$

where $b \ll 1$ is a constant. Equation (2) collapses to Eq. (3) for small signals. Pumping at twice the signal frequency, $\omega_p \sim 2\omega_{s0} = 2\sqrt{(1/L_0 C_0)} \sim 2\omega_s$ leads to a substantial signal gain and eventually to oscillations at the signal frequency.

Numerical results are shown in Fig. 2 for harmonic oscillator type differential equation. The parametrized radial frequency of either Eq. (2) or Eq. (3) was found by using a Mathcad tool. Specifically,

$$d^2 y(t)/dt^2 = -\omega_s^2 y(t) - \kappa dy/dt \quad (4)$$

Here, the radial frequency is related to the frequency as, $\omega_s = 2\pi f_s$ and κ is the loss coefficient. In this semi ideal case, the loss coefficient in the simulations was small but not zero. Larger loss coefficients decrease the intensity of the frequency component. The various coefficients for

the simulations were chosen such that Eq. (2) yields the same coefficients as Eq. (3) when expanding the exponent to first order of approximation. Specifically, when using Eq. 2: $(V_q/R_0 I_0) = 0.01$, $(V_{p0}/V_q) = 2$, and when using Eq. 3: $bV_{p0} = 0.02$. In the case of diode interfaced circuit, higher-order contributions give rise to a large gain in the signal. A fast Fourier transform (fft) module was used to assess the absolute value of the frequency components.

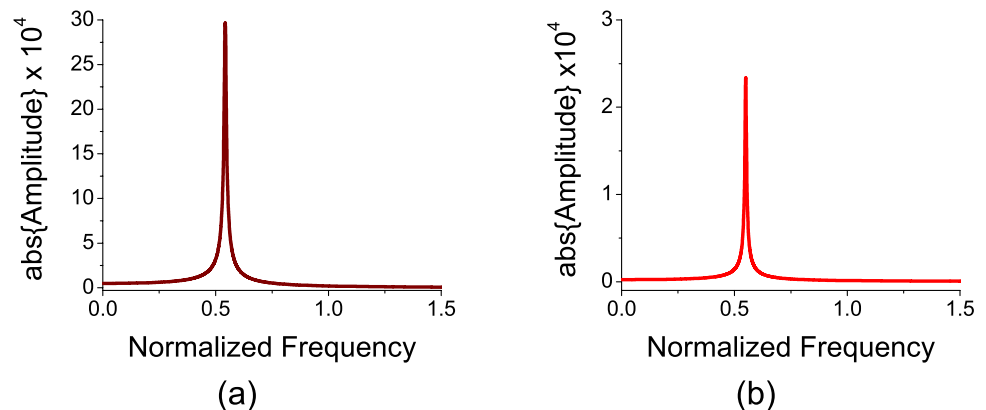
Boundary conditions for the simulations were: $y(0) = 0$ and $(dy(t)/dt)_{t=0} = 2\pi f_0 = 2\pi 0.55$. The normalized pump frequency varies, but it is approximately twice f_0 , namely, $f_p \sim 1.1$. With Eq. 2, the maximum gain is obtained with a somewhat lower or higher pump frequency than when using the pump frequency of Eq. 3. Specifically, in the

case of a parametric oscillator that is driven according to Eq. 3, the maximum gain to the Fourier component is found with $f_p = 1.1$, for which $f_s = 0.55$. In the case of a diode interfaced circuit, the maximum gain to the Fourier component is found with $f_p = 1.085$ for which $f_s = 0.542$ (Fig. 2). The experimental peak frequency also shifts as shown in Fig. 9 below.

In the simulations, a bandwidth of 0.4% of the central pump frequency, or $Q \sim 250$ is noted. The effective parameters, chosen for the comparison between Eqs. 2 and 3 favor a relatively narrow band; these parameters are translated to a large effective circuit resistance, R_0 .

Instead of looking at the leading Fourier component it might be instructive to watch the time evolution of the signal. A typical parametric oscillation, which is driven along with Eq. 3 would exhibit a monotonous, exponentially growing amplitude (Fig. 3b). In the case of a diode interfaced circuit, higher order nonlinearities affect the kinetics of the amplitude. The amplitude of the signal first decreases and then increases (Fig. 3a). Eventually, and as observed in the experiments, its signal grows much faster

Fig. 2 Models: the absolute value of the Fourier component vs the normalized frequency, f. **a** When using Eq. 2: $(V_q/R_0 I_0) = 0.01$ and $(V_{p0}/V_q) = 2$. **b** When using Eq. 3: $bV_{p0} = 0.02$. The larger effect is observed for the highly nonlinear element—the diode case (a)



to provide a larger gain. Simulations also indicate that the amplitude minimum is shifting towards earlier times as the parameter V_q/R_0I_0 increases while keeping V_{p0}/V_q constant. Similar trend is exhibited if we keep V_q/R_0I_0 constant while increasing V_{p0}/V_q ; for example by increasing the pump amplitude, or by decreasing the temperature (and, thus decreasing $V_q = k_B T/q$, with $k_B T$ —the thermal energy and q —the electron charge).

If the capacitance decreases upon a positive pump swing, we may choose a negative sign for the capacitance change. This is the case near the saturation

region or when the diode direction is reversed. Hence, $C = C_0 - \Delta C = C_0(1 - \Delta C/C_0)$ and we get Eq. 5 below,

$$\omega_s^2 \approx (1/L_0 C_0) (1 + (V_q/R_0 I_0) \exp[-(V_{p0}/V_q) \sin(\omega_p t)]) \tag{5}$$

For the simulations, parameters were selected as before: $(V_q/R_0 I_0) = 0.01$ and $(V_{p0}/V_q) = 2$. Maximum gain is achieved with a slightly larger frequency than resonance, $f_p = 1.115$, and the signal is exhibited at $f_s = 0.558$. The Fourier component is now 5 time larger than the one depicted in Fig. 2a and the minimum in the temporal growth has shifted to $t = 0$ (Fig. 4a).

Fig. 3 Normalized amplitudes of the signal as a function of normalized time for: **a** parametric frequency of Eq. 2 and **b** with parametric frequency of Eq. 3. In the harmonic oscillator equation (Eq. 4), the Normalized Amplitude, y multiplies the square of normalized radial frequency of either Eq. 2, or Eq. 3. The normalized time is in units of $1/2\pi f_p$

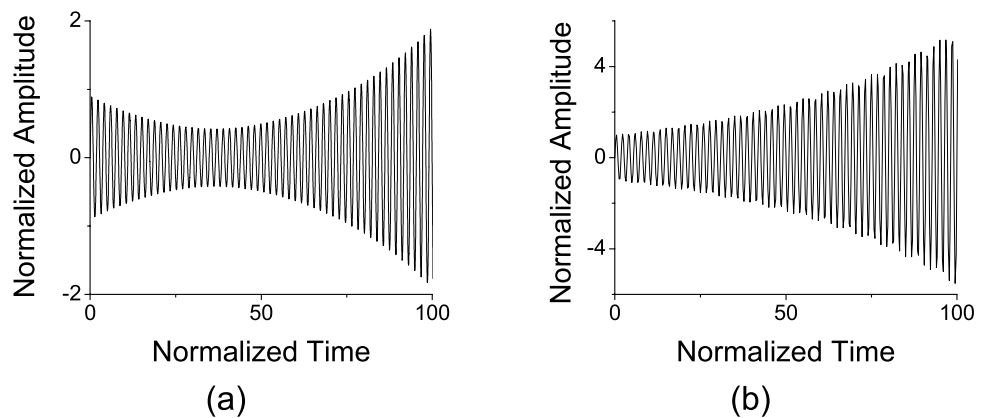


Fig. 4 Models: **a** Time evolution and **b** absolute value of the Fourier component vs the normalized frequency, f when using Eq. 5: $(V_q/R_0 I_0) = 0.01$ and $(V_{p0}/V_q) = 2$

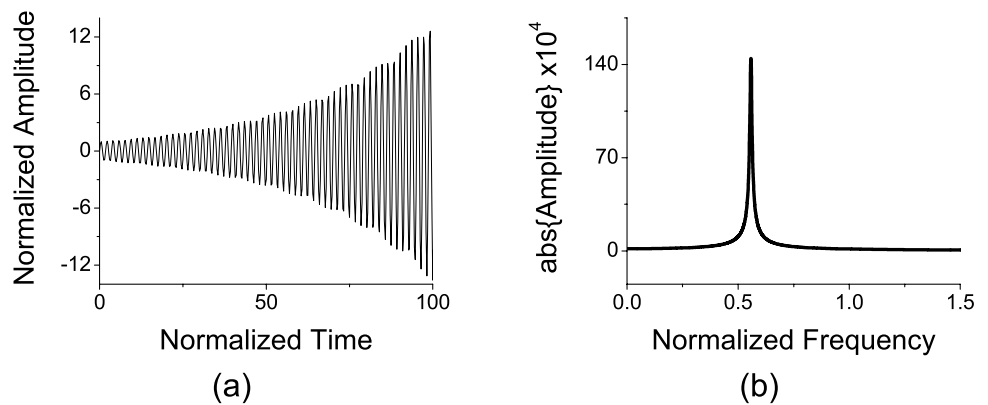
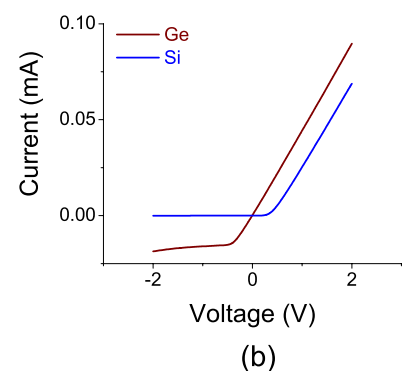
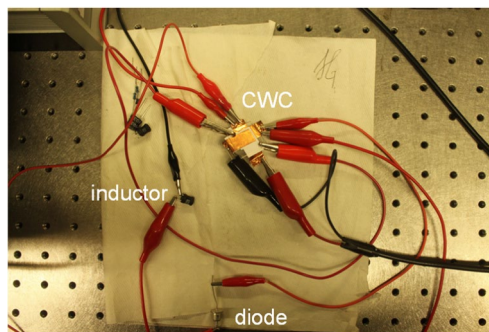


Fig. 5 **a** A picture of the circuit. Four stripes of copper are placed one on top of each other and are separated by dielectric films. The circuit equivalent are provided in Fig. 1b, c. **b** I–V curve of Ge and Si diodes used in the experiments. A third Ge diode, whose I–V is similar to the Si diode, also enabled parametric oscillations. The output voltage V_{out} (Fig. 1b), is assessed with a spectrum analyzer (SA)



3 Methods and experiments

The CWC is made of 4 copper strips (plates), making an area of 12 mm × 12 mm when put across one another (Fig. 5a). They are separated by dielectric films (pieces of cut paper with slightly larger dimensions). The structure is held between two glass slides 25 mm × 25 mm by two clips. The inner gate, which controls the outer cell is operating at resonance with a quality factor of near unity. The capacitance is ca 0.014 nF and ca 0.04 nF between the outer plates and between the inner plates, respectively. The sinusoidal pump frequency is aimed at ca 1.06 MHz; the signal of this degenerate configuration is observed at ca 0.53 MHz (Fig. 6b). The 1N91 1DC723 Ge power diode that connects the gate electrodes has a large reverse breaking voltage rating ($V_R > 75$ V) and a negative break-in voltage (Fig. 6b). Parametric oscillations can be observed with other Ge diodes, as well as with Si diodes (Fig. 5b), though at different DC bias; which is applied to gate electrodes. The entire circuit and layout are shown in Fig. 1c–d. A WaveTek frequency generator, an HP spectrum analyzer (SA) and HP oscilloscope are used to assess the input amplitude, the DC offset and the output spectrum. While the area of the capacitor seems large one should note that the capacitance is quite small due to the distance between the plates. In addition, fringe effect are usually minimized when the capacitor's area is relatively large. Finally, the concept

is general and one may consider other structures, e.g., interdigitated capacitors.

4 Results and discussions

4.1 Experimental results

As with other parametric oscillators, self-oscillation occurs beyond some pump threshold. In Fig. 6a we show the output signals just below the pump threshold; the pump amplitude is 1.8 V_{p-p} . The transmitted output is composed of only the pump frequency at 1.06 MHz. By increasing the pump amplitude to $V_{p-p} = 2$ V and with a DC bias of ca 0.1 V (Fig. 6b), two additional peaks appear: at 0.53 MHz and at 1.59 MHz, respectively. The first peak is the parametric oscillation at half the pump frequency; the second peak is located at the pump frequency and the third one is the peak for the sum frequencies of pump and signal, $\omega_{3p/2} = \omega_p + \omega_s$. The input pump peak intensity was directly measured on the gate (including the inductor and the electrodes' capacitance) as -8.8 dBm for a 2 V_{p-p} amplitude. At threshold, the transmitted signal intensity at either ω_s or $\omega_{3p/2}$ was ca -40 dB of the direct input pump intensity, or -20 dB of the transmitted pump intensity. This is not an optimized configuration: one may achieve a transmitted signal which is only 3 dB below the transmitted pump. An intensity signal-to-noise ratio (SNR) of 40 dB is observed when increasing the input pump power by ca

Fig. 6 **a** Just below threshold. The marker is at 1.06 MHz. **b** Above threshold. Seen is the pump at 1.06 MHz, the signal at 0.53 MHz and the sum of the signal and the pump frequencies at 1.59 MHz. **c** The diode connection is reversed while retaining the same conditions as in **(b)**. The oscillation may be recovered by applying a proper DC bias

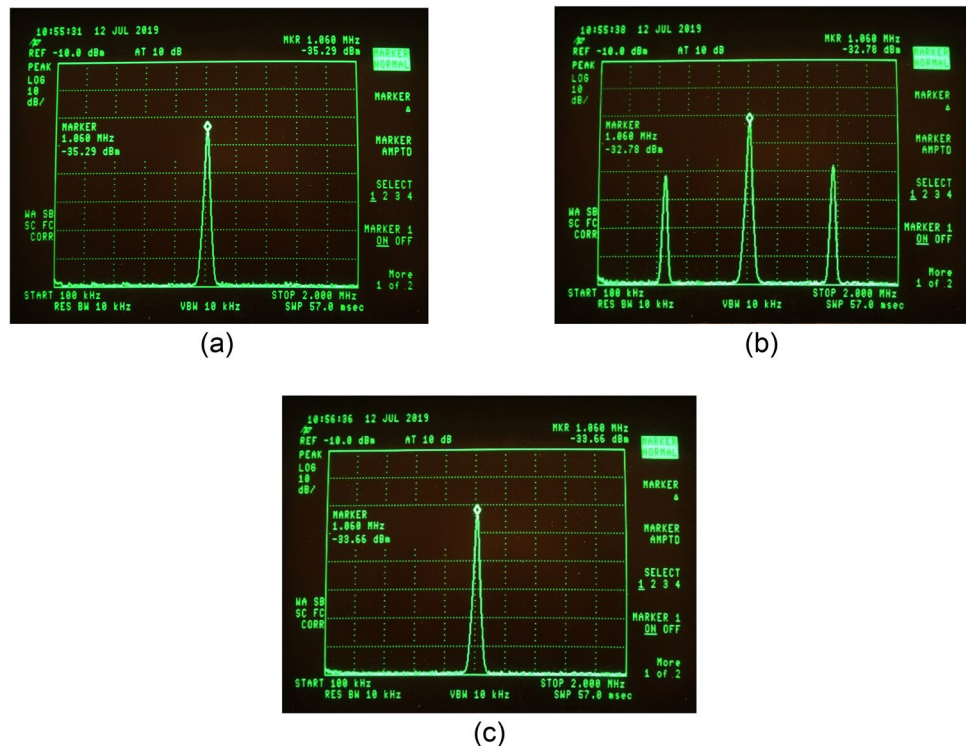
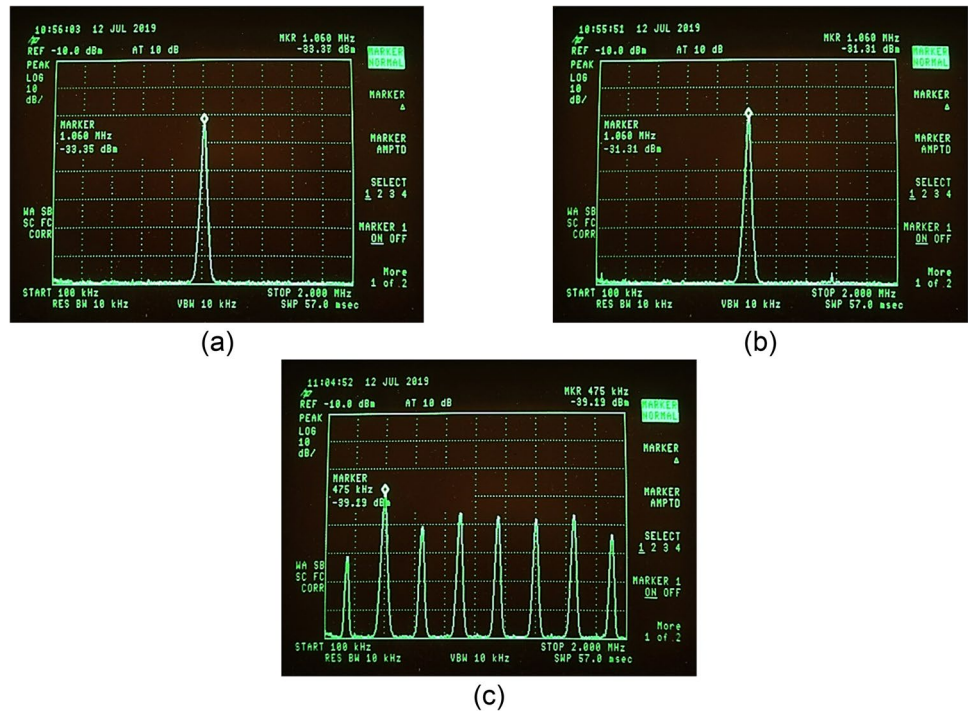


Fig. 7 **a, b** Positive or negative DC offset may suppress the oscillations. **c** Full spectra with harmonics, sub-harmonics and related combinations when the pump frequency is at 0.475 MHz. Note that the pump power is smaller at this lower end of the bandwidth. Here, the DC bias was ~ 0 V



1 dB from just below ($V_{\text{pump}} = 1.8 V_{p-p}$) to just above threshold ($V_{\text{pump}} = 2 V_{p-p}$). Figure 6c shows that the oscillations may be suppressed when reversing the diode connection while retaining the same pump conditions. This means that the polarity of the gate capacitor with respect to the polarity of the cell's capacitor, matters. The oscillations may be recovered with a proper negative or positive DC bias.

Parametric oscillations rely on the nonlinearity of the diode resistance. At large DC bias, the diode exhibits a quasi linear I-V curve and its resistance is almost constant (Fig. 5b). Likewise, when reversed biased, the diode exhibits a constant (and a very large) resistance. These two regions are not appropriate for parametric oscillations. The diode's largest nonlinearity are near the break-in (forward bias), break down (reverse bias) and before the saturation (large forward bias) regions. For a sinusoidal pump amplitude of $< 2 V_{p-p}$, the DC bias range for the Ge diode shown in Fig. 5b is between ± 0.1 V and is optimal for ~ 0 V.

Parametric oscillations may be observed for the above conditions when the pump frequency is scanned between $f = 0.45$ to $f = 1.25$ MHz. Within that frequency range one may observe a rich spectra of sub-harmonics, high pump-frequency's harmonics, as well as combinations between them all (Fig. 7c). Based on that operational frequency range (or, bandwidth), the quality factor

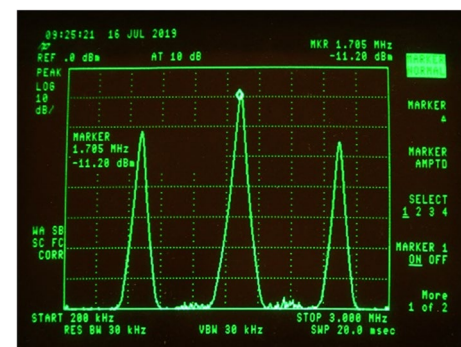
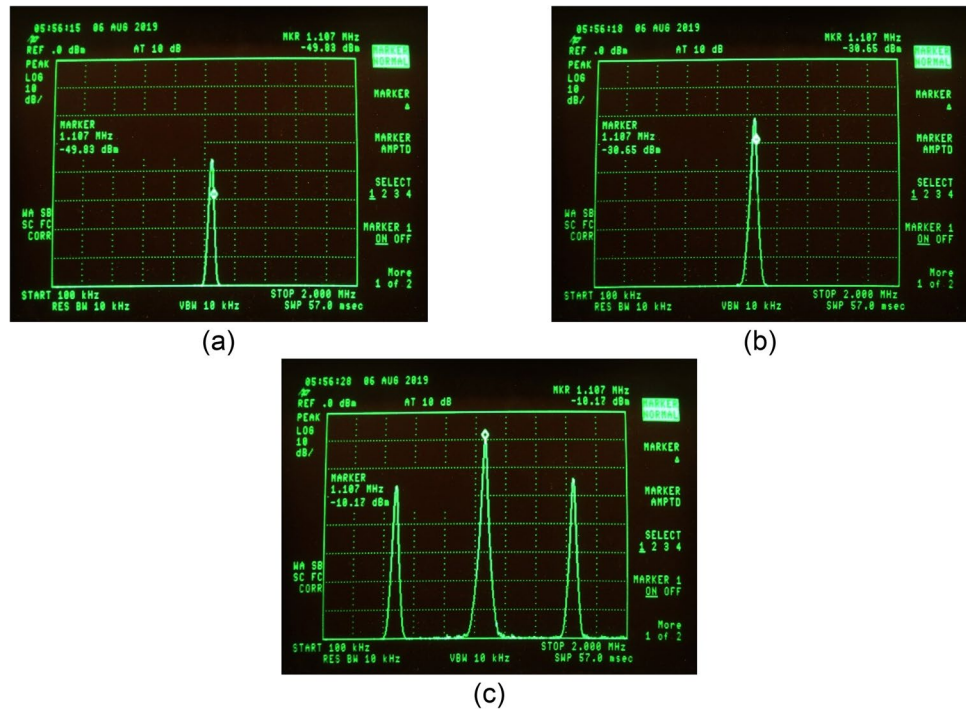


Fig. 8 Higher pump frequencies and broader signals are associated with a larger pump intensities. The signal-to-noise ratio (SNR) is 60 dB

from the pump point of view, $Q = \omega_p / \Delta\omega = 2\pi f_p / 2\pi\Delta f$ is of order 1 (with ω_p chosen at the bandwidth center). The quality factor is also related to the resistance, capacitance and inductance as, $Q = R\sqrt{C/L}$. From the gate point of view, a gate capacitance of ~ 0.04 nF and inductance of 0.22 mH has an effective resistance of, $R_{\text{eff}} \sim 2.3$ KOhms. The impedance of the Ge diode in reverse DC bias is $R_r = 1.5$ KOhms.

Fig. 9 (a–c) As the pump intensity increases throughout the 0–20 V_{p-p} , the pump frequency is up-shifted



What happens if we increase the pump amplitude by 10 times its previous value, say to 20 V_{p-p} or, 20 dB larger than the power threshold? Indeed, the transmitted pump intensity increases by 20 dB (from -30 to -10 dBm); yet, the transmitted signal increases by 30 dB (from -50 to -20 dBm (Fig. 8)). The SNR of the signal is now 60 dB and its peak intensity is only 10 dB below the transmitted peak pump power. As mentioned before, the transmitted signal may reach -3 dB of the transmitted pump at optimized conditions.

Figure 9 shows a pump peak-shift as the pump intensity increases. Clearly, the pump frequency is up-shifting up to the point of oscillation. Similarly, upon changing the value of the inductor from $L = 0.22$ mH to $L = 0.56$ mH the pump frequency is down-shifted (not shown).

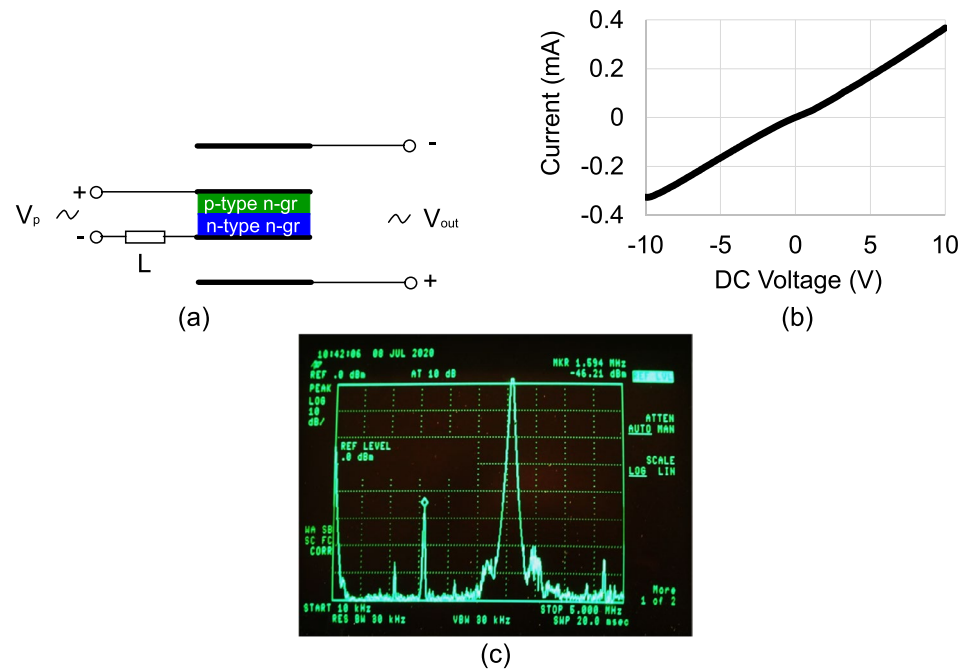
4.2 Ground considerations

If one connects the first and third (negative) electrodes together for a shared ground keeping all other conditions the same, the resonance frequency shifts due to the 50 Ohms resistance of both the functional generator and the spectrum analyzer. A useful frequency range was

experimentally found at lower frequencies ($f_p \sim 600$ kHz and $f_s \sim 300$ kHz).

Graphene may be doped both chemically and electrostatically. The recipe is based on similar approach used for single wall carbon nanotubes [8, 9]. PVP-coated nanographene flakes exhibit p-type film and PEI coated graphene flakes exhibits n-type film. Each of the film type was deposited on a 0.5-nm hole, TS80 membrane and the layout was pressed together. The flakes were soaked in the membrane, let dry out and contact to the film was made through the membrane back. The thickness of the membrane reduced the capacitance of the gate, thus, the resonance of the CWC has increased to ca 3.1 MHz. In Fig. 10 we present the related I–V curve, which exhibits a leaky characteristics. Despite the small nonlinearity of the junction and without the Ge or Si diodes, oscillations were observed (Fig. 10b). They are attributed to the further electrostatic doping of the graphene flakes. The oscillations curve is much narrower than the curve obtained with a standard diode of Fig. 5. The oscillations frequency may be better tuned and do not necessarily occur at $f_{\text{pump}}/2$ but slightly above, or below it.

Fig. 10 **a** Circuit configuration with the nano-graphene (n-gr) gate. The outer cell electrodes are made of copper. **b** I–V curve of a junction made of chemically doped nano-graphene-gr flakes. **c** Related oscillations at $f=1.594$ MHz when pumped at $f=3.1$ MHz



4.3 Amplification

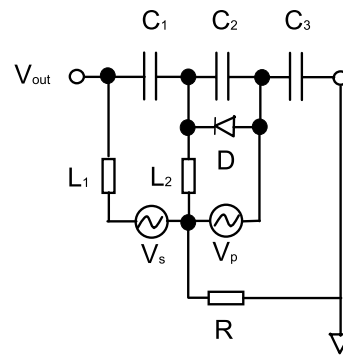
These elements are efficient oscillators and exhibit amplification, as well. The circuit layout is shown in Fig. 11a. We note that the pump and signal channels are separated, which might be attractive for some applications. The transmitted pump intensity was -5 dBm and the intensity of the nonamplified signal was -50.44 dBm. The pump power was adjusted to 1 dB below the onset of oscillations. As observed from Fig. 11, the SNR of the signal was 30 dB and remained so upon amplification to -30.7 dBm (amplification of ca 20 dB). Amplification of 30 dB was achieved when the DC bias, as well as the pump power were adjusted. Finally, oscillations took place upon an increase of the pump power. The resistor R connected the grounds

of the signal (V_s) and the pump (V_p) to the 50 Ohm ground of the spectrum analyzer (V_{out}).

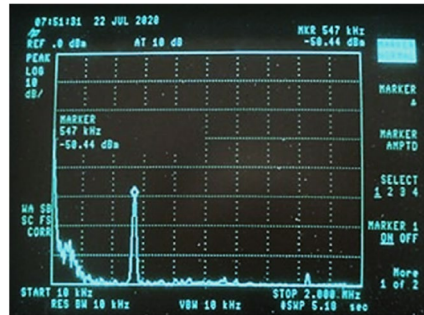
5 Conclusions

A simple and efficient parametric oscillator was built out of a nested structure, a capacitor-within-capacitor (CWC), a diode and an inductor. Higher orders and multiples of frequencies' sum and difference were exhibited due to large diode's nonlinearities [10]. A junction made of chemically doped graphene exhibited oscillations, as well, and may be useful for diode-like, or transistor-like structures, where a voltage bias shifts the Fermi level and hence the electrode's doping. Applications are envisioned with VLSI

Fig. 11 **a** The circuit layout. **b** The signal: -50.44 dBm at 547 kHz. **c** No-signal: the ~ -60 dBm amplifier noise just below the onset of oscillations. **d** The amplified signal at pump— 1 dB below the onset of oscillation and **e** oscillations at pump voltage of $20 V_{p-p}$. $L_1 = L_2 = 0.221$ mH and $R = 0.3$ MOhms. Note that transmitted oscillations are above the transmitted pump



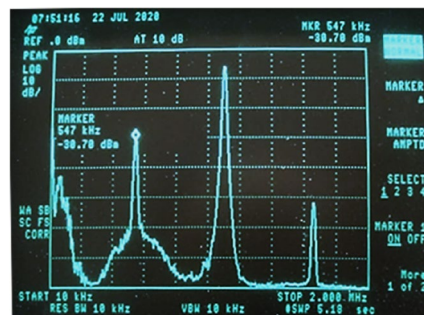
(a)



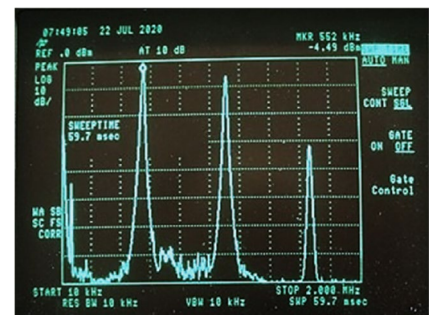
(b)



(c)



(d)



(e)

technology and other capacitor structures, such as travelling waveguide amplifiers and interdigitated electrode capacitors.

Acknowledgements To J. Grebel from U. Chicago for useful comments on the write-up. To T. Chowdhury for help with the nanographene doped junctions.

Availability of data and material Data is available upon reasonable request.

Code availability Code is available upon reasonable request.

Declarations

Conflict of interest The author declares no conflict of interest.

Open Access This article is licensed under a Creative Commons Attribution 4.0 International License, which permits use, sharing, adaptation, distribution and reproduction in any medium or format, as long as you give appropriate credit to the original author(s) and the source, provide a link to the Creative Commons licence, and indicate if changes were made. The images or other third party material in this article are included in the article's Creative Commons licence, unless indicated otherwise in a credit line to the material. If material is not included in the article's Creative Commons licence and your intended use is not permitted by statutory regulation or exceeds the permitted

use, you will need to obtain permission directly from the copyright holder. To view a copy of this licence, visit <http://creativecommons.org/licenses/by/4.0/>.

References

1. Landau LD, Lifshitz EM (1960) *Electrodynamics of continuous media*, vol 8. Pergamon Press
2. Zhu L, Ke Wu (2000) Accurate circuit model of interdigital capacitor and its application to design of new quasi-lumped miniaturized filters with suppression of harmonic resonance. *IEEE Trans Microwave Theory Tech* 48:347–356
3. Grebel H (2019) Capacitor within capacitor. *SN Appl Sci* 1:48. <https://doi.org/10.1007/s42452-018-0058-z>
4. Meric I, Han MY, Young AF, Ozyilmaz B, Kim P, Shepard KL (2008) Current saturation in zero-bandgap, top gated graphene field-effect transistors. *Nat Nanotechnol* 3:654–659
5. Roer TG (2012) *Microwave electronic devices*, vol 10. Springer Science and Business Media
6. Irwin KD, Huber ME (2001) SQUID operational amplifier. *IEEE Trans Appl Supercond* 11(1):1265–1270. <https://doi.org/10.1109/77.919580>
7. Yariv A (1989) *Quantum electronics*, 3rd edn. John Wiley and Sons
8. Chowdhury T, Grebel H (2019) Ion-liquid based supercapacitors with inner gate diode-like separators. *Chem Eng* 3(2):39. <https://doi.org/10.3390/chemengineering3020039>
9. Chowdhury TS, Grebel H (2019) Supercapacitors with electrical gates. *Electrochimica Acta*. <https://doi.org/10.1016/j.electacta.2019.03.222>
10. Boutin S, Toyli DM, Venkatramani AV, Eddins AW, Siddiqi I, Blais A (2017) Effect of higher-order nonlinearities on amplification and squeezing in josephson parametric amplifiers. *Phys Rev Appl* 8:054030

Publisher's Note Springer Nature remains neutral with regard to jurisdictional claims in published maps and institutional affiliations.